STRATEGIES FOR IMPROVING THE RECOVERY TIME OF SEMICONDUCTOR METAL-OXIDE GAS SENSORS

Aliyev Kh.F.
Kokand State
University Master's student

Abstract. The recovery time is, together with sensitivity and selectivity, one of the decisive figures of merit of semiconductor metal-oxide (SMOx) chemiresistors, yet it is frequently the slowest and least optimised parameter. A long recovery limits the duty cycle, prevents continuous real-time monitoring and increases the energy budget of a sensor node. This paper analyses the physical origin of the recovery transient and reviews, within a single quantitative framework, the strategies available to shorten it. We model the recovery as a desorption-limited first-order relaxation whose time constant follows an Arrhenius law; from a linearised representation an effective desorption energy of about 0.62 eV is obtained. We then treat the diffusion-limited regime in porous layers, identify the cross-over between reaction- and diffusion-control, and quantify how operating temperature, noble-metal loading, heterojunction formation, grain-size reduction, light activation and thermal modulation each act on these two limiting times. The contributions are summarised and design rules are proposed for sub-second recovery without sacrificing sensitivity.

Keywords: metal-oxide semiconductor; gas sensor; recovery time; desorption energy; gas diffusion; catalytic spillover; light activation; temperature modulation.

1. Introduction

Semiconductor metal-oxide chemiresistors based on SnO_2, ZnO, WO_3, In_2O_3 and related oxides dominate the gas-sensing market because of their low cost, simple read-out and high sensitivity [1, 2]. A complete sensing cycle, however, consists of two transients: a *response* phase, during which the resistance changes upon gas exposure, and a *recovery* phase, during which the resistance returns to its baseline after the gas is removed. The recovery time, conventionally defined as the interval required to recover 90 % of the baseline signal, is in most devices substantially longer than the response time, and it is the parameter that most often disqualifies an otherwise excellent material from practical use [1, 3].

A slow recovery has three practical consequences. First, it lengthens the measurement duty cycle and prevents continuous real-time monitoring of fluctuating gas concentrations. Second, because recovery is usually accelerated by heating, a slow material forces a higher operating temperature and therefore a higher power consumption, which is critical for battery-powered and Internet-of-Things nodes [15].

Third, incomplete recovery between cycles causes baseline drift and degrades quantitative accuracy. Improving (shortening) the recovery time is therefore a central objective of modern sensor engineering.

The aim of this paper is to give a compact, self-contained and quantitative account of why recovery is slow and how it can be accelerated. We first establish the kinetic model of the recovery transient (Section 2), then analyse the desorption-controlled and diffusion-controlled regimes (Sections 3 and 4), and finally review the material and operational strategies that act on each regime (Section 5), supported by model curves that reproduce the trends reported in the experimental literature [6–14].

2. Kinetics of the Recovery Transient

Consider an n-type SMOx sensor exposed to a reducing gas. During exposure the gas reacts with ionosorbed oxygen, releases trapped electrons and lowers the resistance from its baseline value R_a to a steady value R_g. When the gas is removed, oxygen re-adsorbs, re-traps electrons and the resistance relaxes back to R_a. A representative response/recovery transient is shown in Fig. 1, where the response time t_{res} and the recovery time t_{rec} are marked at the 90 % levels.

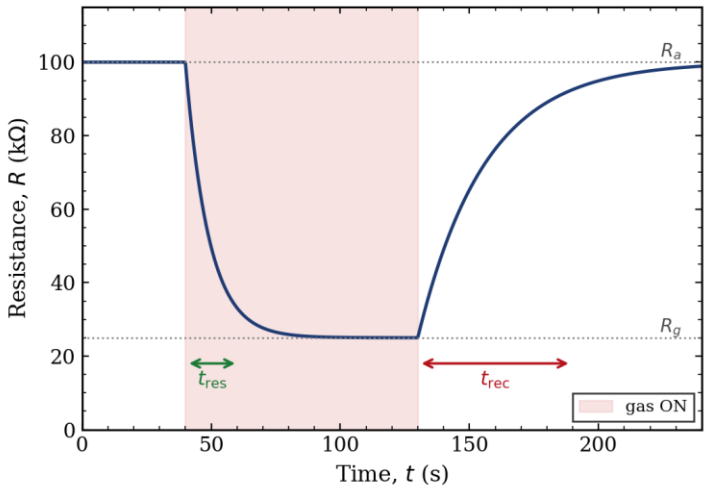

Figure 1. Idealised dynamic response/recovery transient of an n-type SMOx sensor exposed to a reducing gas. The resistance falls from R_a to R^g during exposure (gas ON, shaded) and relaxes back during recovery. t_res and t_rec are defined at the 90 % levels; the recovery branch is markedly slower than the response branch.

The re-oxidation of the surface during recovery is, to first order, a first-order rate process. If θ(t) denotes the fractional coverage of the reduced (electron-rich) surface sites, its relaxation obeys

$$\frac{d\theta}{dt} = -\frac{\theta}{\tau_{rec}} \quad (1)$$

whose solution $\theta(t) = \theta_0 \cdot \exp\left(-\frac{t}{\tau_{rec}}\right)$ translates, through the resistance–coverage relation, into an exponential recovery of the resistance,

$$R(t) = R_a - \left(R_a - R_g\right) exp\left(-\frac{t}{\tau_{rec}}\right) \quad (2)$$

The conventional 90 % recovery time follows directly from Eq. (2) by setting the recovered fraction to 0.9:

$$t_{rec} = \tau_{rec}\, ln\, 10 \approx 2.30\, \tau_{rec} \quad (3)$$

Equation (3) shows that the measurable recovery time is proportional to the underlying relaxation constant τ_{rec}. Any strategy that reduces τ_{rec} therefore shortens the recovery time in direct proportion. Two physical processes set τ_{rec}: (i) the desorption / re-oxidation reaction at the oxide surface, and (ii) the diffusion of gas molecules out of (and oxygen into) the porous sensing layer. The slower of the two controls the recovery; we treat them in turn.

3. Desorption-Limited Recovery and the Activation Energy

When the sensing layer is thin or highly open, gas exchange with the ambient is fast and the recovery is limited by the surface re-oxidation reaction. The relaxation constant is then governed by the desorption rate of the adsorbed analyte, which is thermally activated. Following transition-state theory, τ_{rec} obeys an Arrhenius law,

$$\tau_{rec} = \tau_0\, exp\left(\frac{E_{des}}{k_B T}\right) \quad (4)$$

where τ_0 is the attempt period, E_{des} is the effective desorption (activation) energy of the rate-determining step, k_B is the Boltzmann constant and T the absolute temperature. Equation (4) explains the strong, monotonic decrease of the recovery time with operating temperature seen in Fig. 2: a higher temperature exponentially accelerates desorption, so the surface is cleared more quickly and the baseline is restored faster [4, 5].

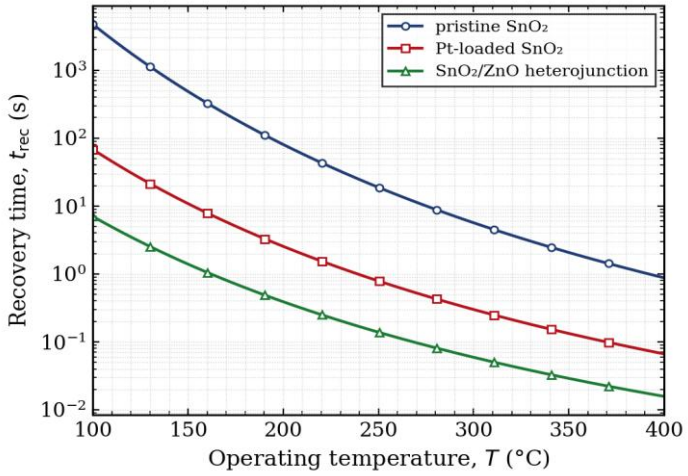

Figure 2. Modelled recovery time t_rec versus operating temperature (logarithmic axis) for pristine SnO_2, Pt-loaded SnO_2 and an SnO_2/ZnO heterojunction. The exponential (Arrhenius) decrease of t_rec with T is the principal lever for acceleration; catalytic and heterojunction modification shift the curves downward by lowering the effective desorption energy.

Taking the natural logarithm of Eq. (4) linearises the dependence on inverse temperature,

$$ln\, t_{rec} \;=\; ln(2.30\,\tau_0) \;+\; \left(\frac{E_{des}}{k_B}\right)\frac{1}{T} \qquad (5)$$

so that a plot of ln t_{rec} against 1/T is a straight line of slope $+E_{des}/k_B$. This Arrhenius construction is the standard route to the desorption energy and is shown in Fig. 3; the linear fit yields $E_{des} \approx 0.62$ eV, a value typical of the re-oxidation of SnO_2-type surfaces and notably larger than the activation energy of the response, which is why recovery is the slower branch [4, 9]. The practical message of Eq. (5) is twofold: recovery can be accelerated either by raising T (moving along a fixed line) or by lowering E_{des} (shifting to a line of smaller slope). The latter is achieved by catalysis.

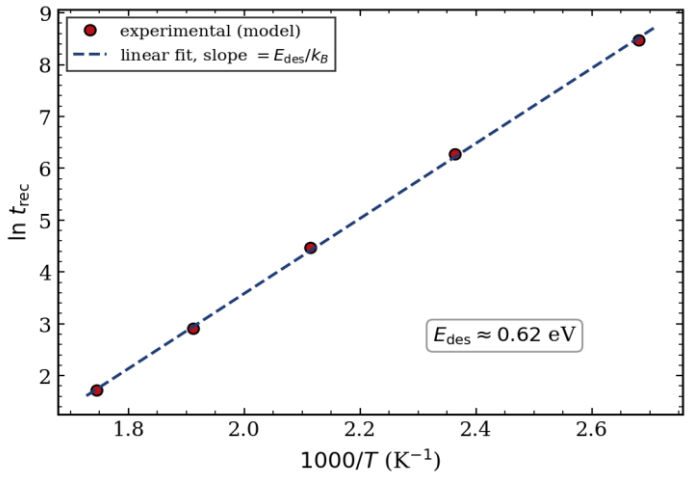

Figure 3. Arrhenius representation of the desorption-limited recovery: ln t_rec versus 1000/T. The positive slope equals +E_des/k_B; the linear fit gives an effective desorption energy E_des ≈ 0.62 eV for the rate-determining re-oxidation step.

4. Diffusion-Limited Recovery in Porous Layers

In thick or densely packed films the recovery may instead be limited by the transport of gas molecules through the porous network rather than by the surface reaction. The characteristic time for a molecule to diffuse out of a layer of thickness L is

$$\tau_{diff} \;\approx\; \frac{L^2}{D_{eff}} \qquad (6)$$

where D_{eff} is the effective diffusion coefficient in the pore system. For mesopores the relevant mechanism is Knudsen diffusion, for which

$$D_K \;=\; \frac{2}{3}\, r_p \sqrt{\frac{8RT}{\pi M}} \qquad (7)$$

with r_p the pore radius, R the gas constant, T the temperature and M the molar mass of the diffusing species. Equations (6)–(7) reveal the geometric levers on the diffusion time: τ_{diff} scales as L^2, so halving the film thickness reduces the diffusion time fourfold, and it scales inversely with the pore radius, so a more open, hierarchically porous structure recovers faster [6, 7, 16]. The competition between the two regimes is captured by the total recovery constant

$$\tau_{rec} \;\approx\; \tau_{des} \;+\; \tau_{diff} \;=\; \tau_0\, exp\left(\frac{E_{des}}{k_B T}\right) \;+\; \frac{L^2}{D_{eff}} \qquad (8)$$

At low temperature the exponential desorption term dominates and recovery is reaction-limited; as the temperature rises this term collapses and the (weakly temperature-dependent) diffusion term takes over. The cross-over defines a practical lower bound on the recovery time that cannot be removed by heating alone and must instead be addressed by morphology engineering. Optimising the recovery therefore requires acting on both terms of Eq. (8) simultaneously: lowering E_{des} through catalysis and minimising L^2/D_{eff} through a thin, open, small-grained microstructure [10, 11].

5. Strategies to Accelerate Recovery

Guided by Eq. (8), the available strategies can be grouped according to which term they reduce. Their typical effect is summarised in Table 1 and compared quantitatively in Fig. 4.

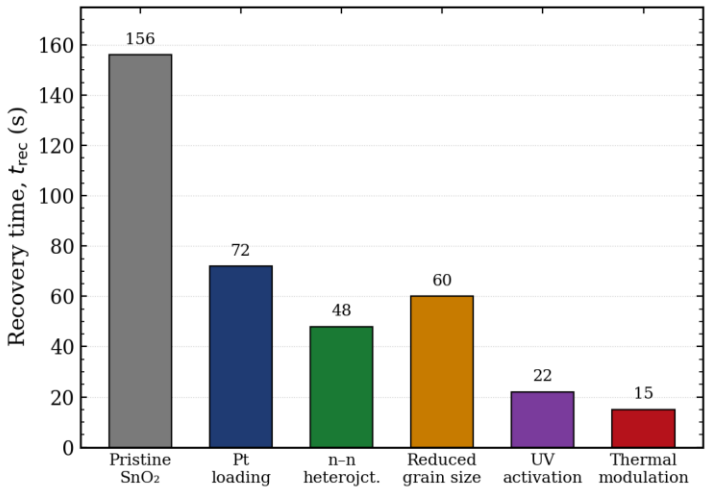

Figure 4. Comparison of the recovery time achieved by different enhancement strategies relative to a pristine SnO_2 baseline (order-of-magnitude model values compiled from [8–14]). Light activation and thermal modulation give the largest reductions because they directly drive desorption.

(a) Elevated operating temperature. Raising T is the most direct lever, since it acts exponentially on the desorption term of Eq. (8). It is, however, paid for by higher power consumption and, beyond the optimum, by reduced sensitivity; it therefore cannot be increased without limit [2, 5].

(b) Noble-metal loading. Decorating the oxide with Pt, Pd or Au nanoparticles lowers E_des through the spillover mechanism: the metal dissociates and channels oxygen, so the surface is re-oxidised more easily after gas removal. This shifts the Arrhenius line of Fig. 3 to a smaller slope and accelerates recovery at a given temperature [8, 9].

(c) Heterojunction engineering. n–n and p–n heterojunctions (e.g. SnO_2/ZnO, CuO/ZnO) provide built-in fields that assist the back-transfer of charge during re-oxidation and supply additional reactive sites, reducing both τ_des and the residual baseline drift [1, 2].

(d) Grain-size and porosity control. Reducing the grain size and creating a hierarchically porous, thin layer attacks the diffusion term L^2/D_{eff} of Eq. (8). When

the grain radius approaches the Debye length the depletion region spans the grain, which simultaneously improves sensitivity and shortens transport paths [10, 11].

(e) Light (UV) activation. Photo-generated electron–hole pairs drive the desorption of surface species at room temperature, providing the activation energy optically rather than thermally. UV illumination therefore yields fast recovery with low power and is especially effective for otherwise sluggish room-temperature oxides [12, 13].

(f) Temperature (pulse) modulation. Applying a short high-temperature pulse after each measurement forces rapid desorption and clears the surface within seconds, while the average power remains low because the pulse duty cycle is small. Combined with self-heating of nanowire elements, this is among the most effective routes to sub-second recovery [14, 15].

Table 1. Strategies for accelerating the recovery of SMOx gas sensors, their typical gain relative to a pristine layer and the dominant physical mechanism (order-of-magnitude values compiled from [8–16]).

Strategy	**Typical t_{rec} gain**	**Dominant mechanism**
Elevated temperature	10×–100×	faster thermal desorption
Noble-metal loading (Pt, Pd, Au)	2×–5×	catalytic spillover, lower E_des
Heterojunction (n–n, p–n)	2×–4×	barrier-assisted charge transfer
Reduced grain / porosity	2×–3×	shorter diffusion length
UV/light activation	3×–10×	photo-desorption at low T
Thermal (pulse) modulation	5×–20×	forced desorption transient

6. Conclusion

The recovery time of a semiconductor metal-oxide gas sensor is set by two competing processes – the thermally activated re-oxidation of the surface and the diffusion of gas through the porous layer – combined in Eq. (8). Modelling the recovery as a first-order desorption relaxation gives the practical relation $t_{rec} \approx 2.30 \cdot \tau_0 \cdot \exp(E_{des}/k_B T)$, from which an Arrhenius analysis yields $E_{des} \approx 0.62$ eV for a typical SnO_2-based layer. Because this desorption energy exceeds that of the response, recovery is intrinsically the slower branch, and accelerating it requires lowering E_{des} (catalysis, heterojunctions, light activation) and minimising the diffusion time L^2/D_{eff} (thin, open, small-grained morphology), supplemented by elevated temperature or pulse modulation. The combined framework presented here, together with the comparison of Table 1 and Fig. 4, provides a coherent set of design rules for achieving fast, sub-second recovery while preserving sensitivity and minimising power consumption – a prerequisite for continuous, real-time and low-power gas monitoring.

References

1. Dutta T., Noushin T., Tabassum S., Mishra S.K. Road map of semiconductor metal-oxide-based sensors: A review. Sensors, 2023, vol. 23, no. 15, 6849.
2. Goel N., Kunal K., Kushwaha A., Kumar M. Metal oxide semiconductors for gas sensing. Engineering Reports, 2023, vol. 5, no. 6, e12604.
3. Liu X., Cheng S., Liu H., Hu S., Zhang D., Ning H. A survey on gas sensing technology. Sensors, 2012, vol. 12, no. 7, pp. 9635–9665.
4. Barsan N., Weimar U. Conduction model of metal oxide gas sensors. Journal of Electroceramics, 2001, vol. 7, no. 3, pp. 143–167.
5. Yamazoe N., Sakai G., Shimanoe K. Oxide semiconductor gas sensors. Catalysis Surveys from Asia, 2003, vol. 7, no. 1, pp. 63–75.
6. Wang X., Wang Y., Tian F., et al. From the surface reaction control to gas-diffusion control: the synthesis of hierarchical porous SnO_2 microspheres and their gas-sensing mechanism. Journal of Physical Chemistry C, 2015, vol. 119, no. 27, pp. 15963–15976.
7. Sakai G., Matsunaga N., Shimanoe K., Yamazoe N. Theory of gas-diffusion controlled sensitivity for thin film semiconductor gas sensor. Sensors and Actuators B, 2001, vol. 80, no. 2, pp. 125–131.
8. Kolmakov A., Klenov D., Lilach Y., Stemmer S., Moskovits M. Enhanced gas sensing by individual SnO_2 nanowires and nanobelts functionalized with Pd catalyst particles. Nano Letters, 2005, vol. 5, no. 4, pp. 667–673.
9. Degler D., Weimar U., Barsan N. Current understanding of the fundamental mechanisms of doped and loaded semiconducting metal-oxide-based gas sensing materials. ACS Sensors, 2019, vol. 4, no. 9, pp. 2228–2249.
10. Korotcenkov G. The role of morphology and crystallographic structure of metal oxides in response of conductometric-type gas sensors. Materials Science and Engineering: R, 2008, vol. 61, no. 1–6, pp. 1–39.
11. Xu C., Tamaki J., Miura N., Yamazoe N. Grain size effects on gas sensitivity of porous SnO_2-based elements. Sensors and Actuators B, 1991, vol. 3, no. 2, pp. 147–155.
12. Comini E., Cristalli A., Faglia G., Sberveglieri G. Light enhanced gas sensing properties of indium oxide and tin dioxide sensors. Sensors and Actuators B, 2000, vol. 65, no. 1–3, pp. 260–263.
13. Chinh N.D., Quang N.D., Lee H., et al. NO gas sensing kinetics at room temperature under UV light irradiation of In_2O_3 nanostructures. Scientific Reports, 2016, vol. 6, 35066.
14. Lee A.P., Reedy B.J. Temperature modulation in semiconductor gas sensing. Sensors and Actuators B, 1999, vol. 60, no. 1, pp. 35–42.

15. Majhi S.M., Mirzaei A., Kim H.W., Kim S.S., Kim T.W. Recent advances in energy-saving chemiresistive gas sensors: A review. Nano Energy, 2021, vol. 79, 105369.
16. Tiemann M. Porous metal oxides as gas sensors. Chemistry – A European Journal, 2007, vol. 13, no. 30, pp. 8376–8388.
17. Barsan N., Weimar U. Understanding the fundamental principles of metal oxide based gas sensors; the example of CO sensing with SnO_2 sensors in the presence of humidity. Journal of Physics: Condensed Matter, 2003, vol. 15, no. 20, R813.
18. Ji H., Zeng W., Li Y. Gas sensing mechanisms of metal oxide semiconductors: A focus review. Nanoscale, 2019, vol. 11, no. 47, pp. 22664–22684.